

Sparse Frequency Analysis with Sparse-Derivative Instantaneous Amplitude and Phase Functions

Yin Ding and Ivan W. Selesnick

Abstract—This paper addresses the problem of expressing a signal as a sum of frequency components (sinusoids) wherein each sinusoid may exhibit abrupt changes in its amplitude and/or phase. The Fourier transform of a narrow-band signal, with a discontinuous amplitude and/or phase function, exhibits spectral and temporal spreading. The proposed method aims to avoid such spreading by explicitly modeling the signal of interest as a sum of sinusoids with time-varying amplitudes. So as to accommodate abrupt changes, it is further assumed that the amplitude/phase functions are approximately piecewise constant (i.e., their time-derivatives are sparse). The proposed method is based on a convex variational (optimization) approach wherein the total variation (TV) of the amplitude functions are regularized subject to a perfect (or approximate) reconstruction constraint. A computationally efficient algorithm is derived based on convex optimization techniques. The proposed technique can be used to perform band-pass filtering that is relatively insensitive to narrow-band amplitude/phase jumps present in data, which normally pose a challenge (due to transients, leakage, etc.). The method is illustrated using both synthetic signals and human EEG data for the purpose of band-pass filtering and the estimation of phase synchrony indexes.

Index Terms—sparse signal representation, total variation, discrete Fourier transform (DFT), instantaneous frequency, phase locking value, phase synchrony.

I. INTRODUCTION

SEVERAL methods in time series analysis aim to quantify the phase behavior of one or more signals (e.g., studies of phase synchrony and coherence among EEG channels [5], [6], [28], [33], [64], [65]). These methods are most meaningfully applied to signals that consist primarily of a single narrow-band component. However, in practice, available data often does not have a frequency spectrum localized to a narrow band, in which case the data is usually band-pass filtered to isolate the frequency band of interest (e.g., [33], [64]). Yet, the process of band-pass filtering has the effect of spreading abrupt changes in phase and amplitude across both time and frequency. Abrupt changes present in the underlying component will be reduced. This limitation of linear time-invariant (LTI) filtering is well recognized. In linear signal analysis, time and frequency resolution can be traded-off with one another (c.f. wavelet transforms); however, they can not both be improved arbitrarily. Circumventing this limitation requires some form of nonlinear signal analysis [14]. The nonlinear analysis method developed in this paper is motivated

by the problem of extracting (isolating) a narrow-band signal from a generic signal while preserving abrupt phase-shifts and amplitude step-changes due for example to phase-resetting [56].

This paper addresses the problem of expressing a signal as a sum of frequency components (sinusoids) wherein each sinusoid may exhibit abrupt changes in its amplitude and/or phase. The discrete Fourier transform (DFT) and Fourier series each give a representation of a generic signal as a sum of sinusoids, wherein the amplitude and phase of each sinusoid is a constant value (not time-varying). In contrast, in the proposed method, the amplitude and phase of each sinusoid is a time-varying function. So as to effectively represent abrupt changes, it is assumed that the amplitude and phase of each sinusoid is approximately constant; i.e., the time-derivative of the amplitude and phase of each sinusoid is sparse. It is further assumed that the signal under analysis admits a sparse frequency representation; i.e., the signal consists of relatively few frequency components (albeit with time-varying amplitudes and phases).

In the proposed sparse frequency analysis (SFA) approach, the amplitude and phase of each sinusoid is allowed to vary so as (i) to match the behavior of data wherein it is known or expected that abrupt changes in amplitude and phase may be present (e.g., signals with phase-reset phenomena), and (ii) to obtain a more sparse signal representation relative to the DFT or oversampled DFT, thereby improving frequency and phase resolution.

The proposed method has a parameter by which one can tune the behavior of the decomposition. At one extreme, the method coincides with the DFT. Hence, the method can be interpreted as a generalization of the DFT.

In order to achieve the above-described signal decomposition, we formulate it as the solution to a convex sparsity-regularized linear inverse problem. Specifically, the total variation (TV) of the amplitude of each sinusoid is regularized. Two forms of the problem are described. In the first form, perfect reconstruction is enforced; in the second form, the energy of the residual is minimized. The second form is suitable when the given data is contaminated by additive noise. The two forms are analogous to basis pursuit (BP) and basis pursuit denoising (BPD) respectively [14].

To solve the formulated optimization problems, iterative algorithms are derived using convex optimization techniques: variable splitting, the alternating direction method of multipliers (ADMM) [3], [7], [15], and majorization-minimization (MM) [21]. The developed algorithms use total variation denoising (TVD) [12], [54] as a sub-step, which is solved exactly

The authors are with the Department of Electrical and Computer Engineering, Polytechnic Institute of New York University, 6 MetroTech Center, Brooklyn, NY 11201. Email: adamding0215@me.com and selesi@poly.edu. Phone: 718 260-3416. Fax: 718 260-3906.

This research was support by the NSF under Grant No. CCF-1018020.

using the recently developed algorithm by Condat [16]. The resulting algorithm is ‘matrix-free’ in that it does not require solving systems of linear equations nor accessing individual rows/columns of matrices.

The proposed signal decomposition can be used to perform mildly nonlinear band-pass filtering that is better able to track abrupt amplitude/phase jumps than an LTI bandpass filter. Such band-pass filtering is also relatively insensitive to narrow-band amplitude/phase jumps present outside the frequency band of interest (interference), which normally pose a challenge (due to transients, leakage, etc.). The method is illustrated using both synthetic signals and human EEG data, for the purpose of band-pass filtering and the estimation of phase synchrony indexes. In the examples, the proposed method is compared with the DFT and with band-pass filtering. The examples demonstrate the improved ability to represent and detect abrupt phase shifts and amplitude changes when they are present in the data.

A. Related work

The short-time Fourier transform (STFT) can already be used to some extent to estimate and track the instantaneous frequency and amplitude of narrow-band components of a generic signal [4], [23], [34]; however, the STFT is computed as a linear transform and is defined in terms of pre-defined basis functions, whereas the proposed representation is computed as the solution to a non-quadratic optimization problem. As discussed in [48], the time-frequency resolution of the STFT is constrained by the utilized window. Hence, although the STFT can be computed with far less computation, it does not have the properties of the proposed approach. On the other hand, the effectiveness and suitability of the proposed approach depends on the validity of the sparsity assumption.

We also note that the sparse STFT (i.e. basis pursuit with the STFT) and other sparse time-frequency distributions can overcome some of the time-frequency limitations of the linear STFT [22]. However, the aim therein is an accurate high resolution time-frequency distribution, whereas the aim of this paper is to produce a representation in the time-domain as a sum of sinusoids with abrupt amplitude/phase shifts.

Sinusoidal modeling also seeks to represent a signal as a sum of sinusoids, each with time-varying amplitude and phase/frequency [35], [37], [43], [44]. However, sinusoidal models usually assume that these are slowly varying functions. Moreover, these functions are often parameterized and the parameters estimated through nonlinear least squares or by short-time Fourier analysis. The goal of this paper is somewhat similar to sinusoidal modeling, yet the model and optimization approach are quite distinct. The method presented here is non-parametric and can be understood as a generalization of the DFT.

Empirical mode decomposition (EMD) [30], a nonlinear data-adaptive approach that decomposes a non-stationary signal into oscillatory components, also seeks to overcome limitations of linear short-time Fourier analysis [1], [51], [52]. In EMD, the oscillatory components, or ‘intrinsic mode functions’ (IMFs), are not restricted to occupy distinct bands. Hence, EMD provides a form of time-frequency analysis. In contrast, the

sparse frequency analysis (SFA) approach presented here is more restrictive in that it assumes the narrow band components occupy non-overlapping frequency bands. EMD, however, is susceptible to a ‘mode mixing’ issue, wherein the instantaneous frequency of an IMF does not accurately track the frequency of the underlying non-stationary component. This is the case, in particular, when the instantaneous amplitude/phase of a component exhibits an abrupt shift. Several optimization-based variations and extensions of EMD have been formulated that aim to provide a more robust and flexible form of EMD [27], [39], [40], [45], [49]. In these methods, as in EMD, one narrow-band component (IMF) is extracted at a time, the frequency support of each component is not constrained a priori, and the instantaneous amplitude/phase of each component is modeled as slowly varying. In contrast, the SFA method developed below, optimizes all components jointly, uses a fixed uniform discretization of frequency, and models the instantaneous amplitude/phase as possessing discontinuities. Hence, SFA and EMD-like methods have somewhat different aims and are most suitable for different types of signals.

Other related works include the synchrosqueezed wavelet transform [17], the iterated Hilbert transform (IHT) [24], and more generally, algorithms for multicomponent AM-FM signal representation (see [25]). These works, again, model the instantaneous amplitudes/phase functions as smooth.

II. PRELIMINARIES

A. Notation

In this paper, vectors and matrices are represented in bold (e.g. \mathbf{x} and \mathbf{D}). Scalars are represented in regular font, e.g., Λ and α .

The N -point sequence $x(n)$, $n \in \mathbb{Z}_N = \{0, \dots, N-1\}$ is denoted as the column vector

$$\mathbf{x} = [x(0), x(1), \dots, x(N-1)]^t. \quad (1)$$

The N -point inverse DFT (IDFT) is given by

$$x(n) = \frac{1}{N} \sum_{k=0}^{N-1} X(k) \exp\left(j \frac{2\pi k}{N} n\right). \quad (2)$$

The IDFT can alternately be expressed in terms of sines and cosines as

$$x(n) = \sum_{k=0}^{N-1} \left(a_k \cos\left(\frac{2\pi k}{N} n\right) + b_k \sin\left(\frac{2\pi k}{N} n\right) \right). \quad (3)$$

We use k to denote the discrete frequency index. The variables $c(n, k)$ and $s(n, k)$ will denote $c(n, k) = \cos(2\pi f_k n)$ and $s(n, k) = \sin(2\pi f_k n)$ for $n \in \mathbb{Z}_N$ and $k \in \mathbb{Z}_K = \{0, \dots, K-1\}$.

When $\mathbf{a} \in \mathbb{R}^{N \times K}$ is an array, we will denote the k -th column by \mathbf{a}_k , i.e.,

$$\mathbf{a} = [\mathbf{a}_0, \mathbf{a}_1, \dots, \mathbf{a}_{K-1}]. \quad (4)$$

The ℓ_1 norm of a vector \mathbf{v} is denoted $\|\mathbf{v}\|_1 = \sum_i |v(i)|$. The energy of a vector \mathbf{v} is denoted $\|\mathbf{v}\|_2^2 = \sum_i |v(i)|^2$.

B. Total Variation Denoising

The total variation (TV) of the discrete N -point signal \mathbf{x} is defined as

$$\text{TV}(\mathbf{x}) = \sum_{n=1}^{N-1} |x(n) - x(n-1)|. \quad (5)$$

The TV of a signal is a measure of its temporal fluctuation. It can be expressed as

$$\text{TV}(\mathbf{x}) = \|\mathbf{D}\mathbf{x}\|_1 \quad (6)$$

where \mathbf{D} is the matrix

$$\mathbf{D} = \begin{bmatrix} -1 & 1 & & & & & & & \\ & -1 & 1 & & & & & & \\ & & & \ddots & \ddots & & & & \\ & & & & & -1 & 1 & & \\ & & & & & & & -1 & 1 \end{bmatrix} \quad (7)$$

of size $(N-1) \times N$. That is, $\mathbf{D}\mathbf{x}$ denotes the first-order difference of signal \mathbf{x} .

Total Variation Denoising (TVD) [54] is a nonlinear filtering method defined by the convex optimization problem,

$$\text{tvd}(\mathbf{y}, \lambda) := \arg \min_{\mathbf{x}} \|\mathbf{y} - \mathbf{x}\|_2^2 + \lambda \|\mathbf{D}\mathbf{x}\|_1 \quad (8)$$

where \mathbf{y} is the noisy signal and $\lambda > 0$ is a regularization parameter. We denote the output of the TVD denoising problem by $\text{tvd}(\mathbf{y}, \lambda)$ as in (8). Specifying a large value for the regularization parameter λ increases the tendency of the denoised signal to be piece-wise constant.

Efficient algorithms for 1D and multidimensional TV denoising have been developed [11], [13], [42], [53], [61] and applied to several linear inverse problems arising in signal and image processing [19], [20], [41], [55], [62]. Recently, a fast and exact algorithm has been developed [16].

III. SPARSE FREQUENCY ANALYSIS

As noted in the Introduction, we model the N -point signal of interest, $\mathbf{x} \in \mathbb{R}^N$, as a sum of sinusoids, each with a time-varying amplitude and phase. Equivalently, we can write the signal as a sum of sines and cosines, each with a time-varying amplitude and zero phase. Hence, we have the signal representation:

$$x(n) = \sum_{k=0}^{K-1} \left(a_k(n) \cos(2\pi f_k n) + b_k(n) \sin(2\pi f_k n) \right) \quad (9)$$

where $f_k = k/K$ and $a_k(n), b_k(n) \in \mathbb{R}$, $k \in \mathbb{Z}_K$, $n \in \mathbb{Z}_N$.

The expansion (9) resembles the real form of the inverse DFT (3). However, in (9) the amplitudes a_k and b_k are time-varying. As a consequence, there are $2NK$ coefficients in (9), in contrast to $2N$ coefficients in (3).

In addition, note that the IDFT is based on N frequencies, where N is the signal length. In contrast, the number of frequencies K in (9) can be less than the signal length N . Because there are $2KN$ independent coefficients in (9), the signal \mathbf{x} can be perfectly represented with fewer than N frequencies ($K < N$).

In fact, with $K = 1$, we can take $a_0(n) = x(n)$ and $b_0(n) = 0$ and satisfy (9) with equality. [With $K = 1$, the only term

in the sum is $a_0(n) \cos(2\pi f_0 n)$ with $f_0 = 0$.] However, this solution is uninteresting – the aim being to decompose $x(n)$ into a set of sinusoids (and cosines) with approximately piecewise constant amplitudes.

With $K > 1$, there are infinitely many solutions to (9). In order to obtain amplitude functions $a_k(n)$ and $b_k(n)$ that are approximately piecewise constant, we regularize the total variation of $\mathbf{a}_k \in \mathbb{R}^N$ and $\mathbf{b}_k \in \mathbb{R}^N$ for each $k \in \mathbb{Z}_K$, where \mathbf{a}_k denotes the N -point amplitude sequence of the k -th cosine component, i.e., $\mathbf{a}_k = (a_k(n))_{n \in \mathbb{Z}_N}$. Similarly, \mathbf{b}_k denotes the N -point amplitude sequence of the k -th sine component. Regularizing $\text{TV}(\mathbf{a}_k)$ and $\text{TV}(\mathbf{b}_k)$ promotes sparsity of the derivatives (first-order difference) of \mathbf{a}_k and \mathbf{b}_k , as is well known. Note that $\text{TV}(\mathbf{a}_k)$ can be written as $\|\mathbf{D}\mathbf{a}_k\|_1$. This notation will be used below.

It is not sufficient to regularize $\text{TV}(\mathbf{a}_k)$ and $\text{TV}(\mathbf{b}_k)$ only. Note that if $a_k(n)$ and $b_k(n)$ are not time-varying, i.e., $a_k(n) = \bar{a}_k$ and $b_k(n) = \bar{b}_k$, then $\text{TV}(\mathbf{a}_k) = 0$ and $\text{TV}(\mathbf{b}_k) = 0$. Moreover, a non-time-varying solution of this form in fact exists and is given by the DFT coefficients, c.f. (3). This is true, provided $K \geq N$. That is, based on the DFT, a set of constant-amplitude sinusoids can always be found so as to perfectly represent the signal $x(n)$. The disadvantage of such a solution, as noted in the Introduction, is that if $x(n)$ contains a narrow-band component with amplitude/phase discontinuities (in addition to other components), then many frequency components are needed for the representation of the narrow-band component; i.e., its energy is spectrally spread. (In turn, due to each sinusoid having a constant amplitude, the energy is temporally spread as well.) In this case, the narrow-band component can not be well isolated (extracted) from the signal $x(n)$ for the purpose of further processing or analysis (e.g., phase synchronization index estimation).

Therefore, in addition to regularizing only the total variation of the amplitudes, we also regularize the frequency spectrum corresponding to the representation (9). We define the frequency spectrum, z_k , as

$$|z_k|^2 = \sum_n |a_k(n)|^2 + |b_k(n)|^2, \quad k \in \mathbb{Z}_K \quad (10)$$

or equivalently

$$|z_k|^2 = \|\mathbf{a}_k\|_2^2 + \|\mathbf{b}_k\|_2^2, \quad k \in \mathbb{Z}_K. \quad (11)$$

The frequency-indexed sequence z_k measures the distribution of amplitude energy as a function of frequency. Note that, in case the amplitudes are not time-varying, i.e., $a_k(n) = \bar{a}_k$ and $b_k(n) = \bar{b}_k$, then $|z_k|$ represents the modulus of the k -th DFT coefficient. We define the vector $\mathbf{z} \in \mathbb{R}^K$ as $\mathbf{z} = (z_k)_{k \in \mathbb{Z}_K}$. In order to induce \mathbf{z} to be sparse, we regularize its ℓ_1 norm, i.e.,

$$\|\mathbf{z}\|_1 = \sum_{k=0}^{K-1} \sqrt{\|\mathbf{a}_k\|_2^2 + \|\mathbf{b}_k\|_2^2}. \quad (12)$$

According to the preceding discussion, we regularize the total variation of the amplitude functions and the ℓ_1 norm of the frequency spectrum subject to the perfect reconstruction constraint. This is expressed as the optimization problem:

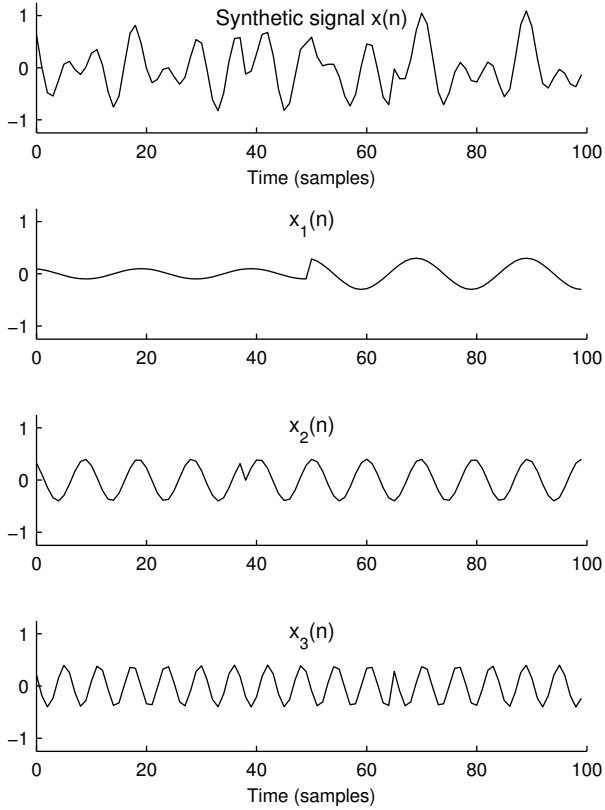


Fig. 1. Example 1: Test signal synthesized as the sum of three sinusoids each with a amplitude/phase discontinuity.

$$\begin{aligned} & \min_{\mathbf{a}, \mathbf{b}} \sum_{k=0}^{K-1} \left(\|\mathbf{D}\mathbf{a}_k\|_1 + \|\mathbf{D}\mathbf{b}_k\|_1 + \lambda \sqrt{\|\mathbf{a}_k\|_2^2 + \|\mathbf{b}_k\|_2^2} \right) \\ \text{s. t. } & x(n) = \sum_{k=0}^{K-1} \left(a(n, k) c(n, k) + b(n, k) s(n, k) \right) \quad (\text{P0}) \end{aligned}$$

where $\lambda > 0$ is a regularization parameter, and where $\mathbf{a}, \mathbf{b} \in \mathbb{R}^{N \times K}$ with $\mathbf{a} = (a(n, k))_{n \in \mathbb{Z}_N, k \in \mathbb{Z}_K}$, and $\mathbf{a}_k, \mathbf{b}_k \in \mathbb{R}^N$ with $\mathbf{a}_k = (a(k, n))_{n \in \mathbb{Z}_N}$. The $c(n, k)$ and $s(n, k)$ denote the cosine and sine terms, $c(n, k) = \cos(2\pi f_k n)$ and $s(n, k) = \sin(2\pi f_k n)$, where $f_k = k/K$.

Notice in (P0), that λ adjusts the relative weighting between the two regularization terms. If $K \geq 2N$, then as $\lambda \rightarrow 0$, the minimization problem leads to a solution approaching $\|\mathbf{D}\mathbf{a}_k\|_1 = \|\mathbf{D}\mathbf{b}_k\|_1 = 0$ for all frequencies $k \in \mathbb{Z}_K$. In this case, \mathbf{a}_k and \mathbf{b}_k are non-time-varying. When $K = 2N$, they coincide with the DFT coefficients, specifically, $K(a_k(n) - jb_k(n))$ is equal to the DFT coefficient $X(k)$ in (2).

A. Example 1: A Synthetic Signal

A synthetic signal $x(n)$ of length $N = 100$ is illustrated in Fig. 1. The signal is formed by adding three sinusoidal components, $x_i(n)$, $i = 1, 2, 3$, with normalized frequencies 0.05, 0.1025 and 0.1625 cycles/sample, respectively. However, each of the three sinusoidal components possess a phase discontinuity ('phase jump') at $n = 50, 38$, and 65 , respectively. The first component, $x_1(n)$, has a discontinuity in both its amplitude and phase.

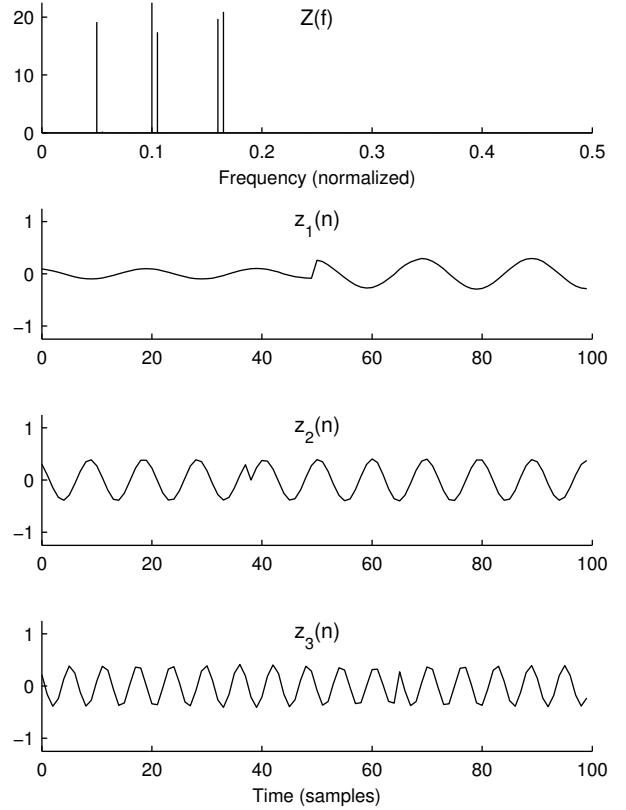


Fig. 2. Example 1: Signal decomposition using sparse frequency analysis (SFA). The frequency spectrum is sparse and the recovered sinusoidal components accurately retain the amplitude/phase discontinuities.

Here, we set $K = 100$, so the uniformly-spaced frequencies f_k , $k \in \mathbb{Z}_K$, from 0 to 0.5, are separated by 0.005 cycles/sample. The frequency grid is similar to that of a 200-point DFT (including zero-padded). The component x_1 lies exactly on the frequency grid, i.e. $0.05 = 10 \times 0.005$. On the other hand, the frequencies of components x_2 and x_3 lie exactly halfway between frequency grid points, i.e., $0.1025 = 20.5 \times 0.005$ and $0.1625 = 32.5 \times 0.005$. The frequencies of x_2 and x_3 are chosen as such so as to test the proposed algorithm under frequency mismatch conditions.

Using the iterative algorithm developed below, we obtain $a(n, k)$ and $b(n, k)$ solving the optimization problem (P0). The frequency spectrum, z_k , defined by (11), is illustrated in Fig. 2. The frequency spectrum is clearly sparse. The component x_1 is represented by a single line in the frequency spectrum at $k = 10$. Note that, because the components x_2 and x_3 of the synthetic test signal are not aligned with the frequency grid, they are each represented by a pair of lines in the frequency spectrum, at $k = (20, 21)$ and $k = (32, 33)$, respectively. This is similar to the leakage phenomena of the DFT, except here, the leakage is confined to two adjacent frequency bins instead of being spread across many frequency bins.

To extract a narrow-band signal from the proposed decomposition, defined by the arrays (\mathbf{a}, \mathbf{b}) , we simply reconstruct the signal using a subset of frequencies, i.e.,

$$g_S(n) = \sum_{k \in S} \left(a(n, k) c(n, k) + b(n, k) s(n, k) \right) \quad (13)$$

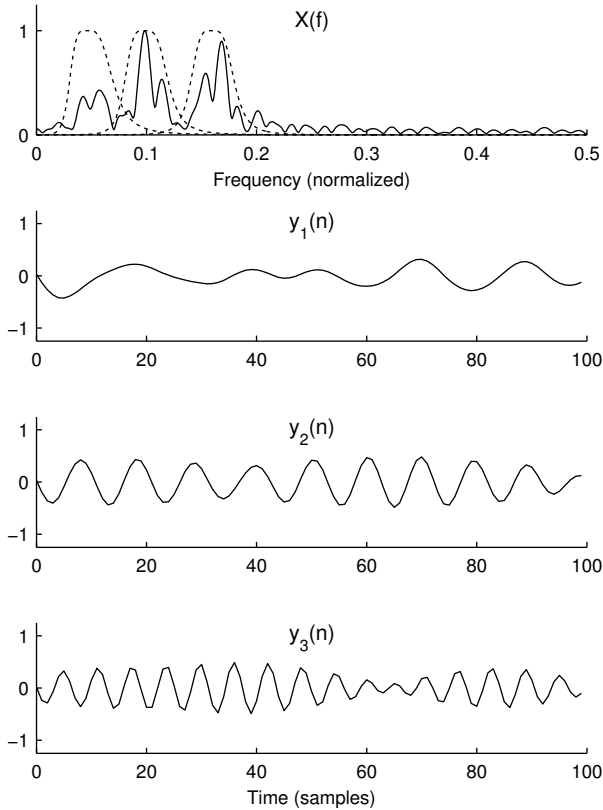


Fig. 3. Example 1: Signal components obtained by LTI band-pass filtering. The Fourier transform $X(f)$ is not sparse and the filtered components do not retain the amplitude/phase discontinuities. The amplitude/phase discontinuities are spread across time and frequency.

where $S \subset \mathbb{Z}_K$ is a set of one or several frequency indices. With $S = \{10\}$, we recover a good approximation of x_1 . With $S = \{20, 21\}$ and $S = \{32, 33\}$, we recover good approximations of components x_2 and x_3 , respectively. These approximations are illustrated in Fig. 2. Note, in particular, that the recovered components retain the amplitude and phase discontinuities present in the original components $x_i(n)$. In other words, from the signal $x(n)$, which contains a mixture of sinusoidal components each with amplitude/phase discontinuities, we are able to recover the components with high accuracy, including their amplitude/phase discontinuities.

Let us compare the estimation of components x_i from x using the proposed method with what can be obtained by band-pass filtering. Band-pass filtering is widely used to analyze components of signals, e.g., analysis of event-related potentials (ERPs) by filtering EEG signals [18], [31]. By band-pass filtering signal x using three band-pass filters, H_i , $i = 1, 2, 3$, we obtain the three output signals, y_i , illustrated in Fig. 3. The band-pass filters are applied using forward-backward filtering to avoid phase distortion. Clearly, the amplitude/phase discontinuities are not well preserved. The point in each output signal, where a discontinuity is expected, exhibits an attenuation in amplitude. The amplitude/phase discontinuities have been spread across time and frequency.

The frequency responses of the three filters we have used are indicated in Fig. 3, which also shows the Fourier transform $|X(f)|$ of the signal $x(n)$. Unlike the frequency spectrum in

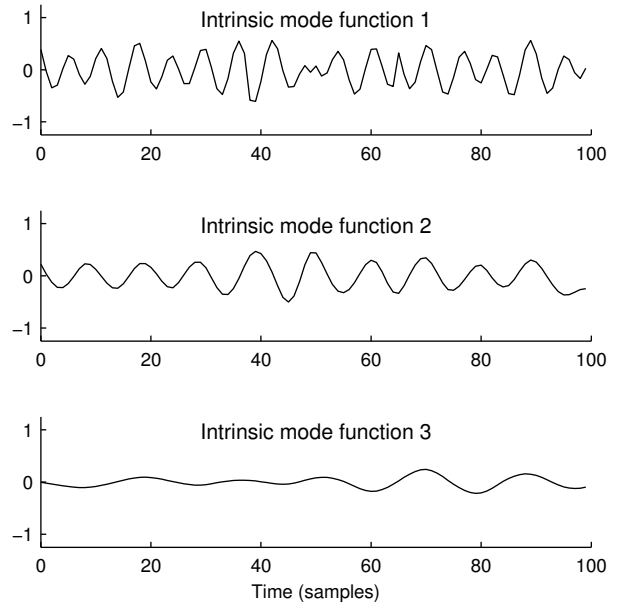


Fig. 4. Example 1: Signal decomposition with the empirical mode decomposition (EMD). The first three intrinsic mode functions (IMFs). The amplitude/phase discontinuities are not preserved.

Fig. 2, the Fourier transform in Fig. 3 is not sparse.

We also compare SFA and band-pass filtering with empirical mode decomposition (EMD) [30]. EMD is a data-adaptive algorithm that decomposes a signal into a set of zero-mean oscillatory components called intrinsic mode functions (IMFs) and a low frequency residual. For the test signal (Fig. 1a), the first three IMFs are illustrated in Fig. 4. (The EMD calculation was performed using the Matlab program `emd.m` from <http://perso.ens-lyon.fr/patrick.flandrin/emd.html> [52].)

Note that the IMFs do not capture the amplitude/phase discontinuities. This is expected, as EMD is based on different assumptions regarding the behavior of the narrow-band components (smooth instantaneous amplitude/phase functions).

Comparing the sparse frequency analysis (SFA) results in Fig. 2 with the band-pass filtering results in Fig. 3 and the EMD results in Fig. 4, it is clear that the SFA method is better able to extract the narrow-band components while preserving abrupt changes in amplitude and phase.

B. Optimization Algorithm

In this section we derive an algorithm for solving problem (P0). We use the alternating direction method of multipliers (ADMM) and the majorization-minimization (MM) method to transform the original problem into a sequence of simpler optimization problems, which are solved iteratively, until convergence to the solution.

By variable splitting, problem (P0) can be written as:

$$\min_{\mathbf{a}, \mathbf{b}, \mathbf{u}, \mathbf{v}} \sum_{k=0}^{K-1} \left(\|\mathbf{D}\mathbf{a}_k\|_1 + \|\mathbf{D}\mathbf{b}_k\|_1 \right) + \lambda \sum_{k=0}^{K-1} \sqrt{\|\mathbf{u}_k\|_2^2 + \|\mathbf{v}_k\|_2^2}$$

$$\text{s. t. } x(n) = \sum_{k=0}^{K-1} \left(u(n, k) c(n, k) + v(n, k) s(n, k) \right) \quad (14a)$$

$$\mathbf{u} = \mathbf{a} \quad (14b)$$

$$\mathbf{v} = \mathbf{b} \quad (14c)$$

where $\mathbf{u}, \mathbf{v} \in \mathbb{R}^{N \times K}$ correspond to matrices \mathbf{a} and \mathbf{b} .

The augmented Lagrangian [2] is given by

$$\begin{aligned} L_0(\mathbf{a}, \mathbf{b}, \mathbf{u}, \mathbf{v}, \lambda, \mu) &= \sum_{k=0}^{K-1} \left(\|\mathbf{D}\mathbf{a}_k\|_1 + \|\mathbf{D}\mathbf{b}_k\|_1 + \lambda \sqrt{\|\mathbf{u}_k\|_2^2 + \|\mathbf{v}_k\|_2^2} \right. \\ &\quad \left. + \mu \|\mathbf{u}_k - \mathbf{a}_k - \mathbf{p}_k\|_2^2 + \mu \|\mathbf{v}_k - \mathbf{b}_k - \mathbf{q}_k\|_2^2 \right) \quad (15) \end{aligned}$$

where $\mu > 0$ is a parameter to be specified, and where the equality constraint (14a) still holds. The parameter μ does not influence the minimizer of cost function (P0). Therefore, the solution of (15) leads to the solution of (P0). The use of ADMM yields the iterative algorithm:

$$\begin{aligned} \mathbf{a}, \mathbf{b} \leftarrow \arg \min_{\mathbf{a}, \mathbf{b}} \sum_{k=0}^{K-1} \left(\|\mathbf{D}\mathbf{a}_k\|_1 + \|\mathbf{D}\mathbf{b}_k\|_1 \right. \\ \left. + \mu \|\mathbf{u}_k - \mathbf{a}_k - \mathbf{p}_k\|_2^2 + \mu \|\mathbf{v}_k - \mathbf{b}_k - \mathbf{q}_k\|_2^2 \right) \quad (16a) \end{aligned}$$

$$\begin{aligned} \mathbf{u}, \mathbf{v} \leftarrow \arg \min_{\mathbf{u}, \mathbf{v}} \sum_{k=0}^{K-1} \left(\lambda \sqrt{\|\mathbf{u}_k\|_2^2 + \|\mathbf{v}_k\|_2^2} \right. \\ \left. + \mu \|\mathbf{u}_k - \mathbf{a}_k - \mathbf{p}_k\|_2^2 + \mu \|\mathbf{v}_k - \mathbf{b}_k - \mathbf{q}_k\|_2^2 \right) \end{aligned}$$

$$\text{s. t. } x(n) = \sum_{k=0}^{K-1} \left(u(n, k) c(n, k) + v(n, k) s(n, k) \right) \quad (16b)$$

$$\mathbf{p} \leftarrow \mathbf{p} - (\mathbf{u} - \mathbf{a}) \quad (16c)$$

$$\mathbf{q} \leftarrow \mathbf{q} - (\mathbf{v} - \mathbf{b}) \quad (16d)$$

$$\text{Go back to (16a).} \quad (16e)$$

In (16a), the variables \mathbf{a} and \mathbf{b} are uncoupled. Furthermore, each of the K columns \mathbf{a}_k and \mathbf{b}_k of \mathbf{a} and \mathbf{b} are decoupled. Hence, we can write

$$\mathbf{a}_k \leftarrow \arg \min_{\mathbf{a}_k} \|\mathbf{D}\mathbf{a}_k\|_1 + \mu \|\mathbf{u}_k - \mathbf{a}_k - \mathbf{p}_k\|_2^2 \quad (17a)$$

$$\mathbf{b}_k \leftarrow \arg \min_{\mathbf{b}_k} \|\mathbf{D}\mathbf{b}_k\|_1 + \mu \|\mathbf{v}_k - \mathbf{b}_k - \mathbf{q}_k\|_2^2 \quad (17b)$$

for $k \in \mathbb{Z}_K$. Problems (17) are recognized as N -point TV denoising problems, readily solved by [16]. Hence we write

$$\mathbf{a}_k \leftarrow \text{tvd}(\mathbf{u}_k - \mathbf{p}_k, 1/\mu) \quad (18a)$$

$$\mathbf{b}_k \leftarrow \text{tvd}(\mathbf{v}_k - \mathbf{q}_k, 1/\mu) \quad (18b)$$

for $k \in \mathbb{Z}_K$.

Problem (16b) can be written as:

$$\begin{aligned} \mathbf{u}, \mathbf{v} \leftarrow \arg \min_{\mathbf{u}, \mathbf{v}} \sum_{k=0}^{K-1} \left[\lambda \sqrt{\sum_{n=0}^{N-1} |u(n, k)|^2 + |v(n, k)|^2} \right. \\ \left. + \mu \sum_{n=0}^{N-1} |u(n, k) - a(n, k) - p(n, k)|^2 \right. \end{aligned}$$

$$\left. + \mu \sum_{n=0}^{N-1} |v(n, k) - b(n, k) - q(n, k)|^2 \right]$$

$$\text{s. t. } x(n) = \sum_{k=0}^{K-1} \left(u(n, k) c(n, k) + v(n, k) s(n, k) \right) \quad (19)$$

which does not admit an explicit solution. Here we use the MM procedure for solving (19), i.e., (16b). First we need a majorizer. To that end, note that for each $k \in \mathbb{Z}_K$,

$$\begin{aligned} \sqrt{\sum_{n=0}^{N-1} |u(n, k)|^2 + |v(n, k)|^2} \\ \leq \frac{1}{2\Lambda_k^{(i)}} \sum_{n=0}^{N-1} (|u(n, k)|^2 + |v(n, k)|^2) + \frac{1}{2}\Lambda_k^{(i)} \quad (20) \end{aligned}$$

where

$$\Lambda_k^{(i)} = \sqrt{\sum_{n=0}^{N-1} |u^{(i)}(n, k)|^2 + |v^{(i)}(n, k)|^2}. \quad (21)$$

Here i is the iteration index for the MM procedure and the right-hand side of (20) is the majorizer. An MM algorithm for solving (19) is hence given by:

$$\begin{aligned} \mathbf{u}^{(i+1)}, \mathbf{v}^{(i+1)} \\ \leftarrow \arg \min_{\mathbf{u}, \mathbf{v}} \sum_{k=0}^{K-1} \left[\sum_{n=0}^{N-1} \left(\frac{\lambda}{2\Lambda_k^{(i)}} (|u(n, k)|^2 + |v(n, k)|^2) \right. \right. \\ \left. \left. + \mu |u(n, k) - a(n, k) - p(n, k)|^2 \right. \right. \\ \left. \left. + \mu |v(n, k) - b(n, k) - q(n, k)|^2 \right) \right] \\ \text{s. t. } x(n) = \sum_{k=0}^{K-1} \left(u(n, k) c(n, k) + v(n, k) s(n, k) \right). \quad (22) \end{aligned}$$

The majorizer is significantly simpler to minimize. With the use of the quadratic term to majorize the ℓ_2 -norm, the problem becomes separable with respect to n . That is, (22) constitutes N independent least-square optimization problems. Moreover, each least-square problem is relatively simple and admits an explicit solution. Omitting straightforward details, $\mathbf{u}^{(i+1)}$ and $\mathbf{v}^{(i+1)}$ solving (22) are given explicitly by:

$$\begin{aligned} u^{(i+1)}(n, k) = V_k \left[\alpha(n, k) c(n, k) \right. \\ \left. + 2\mu(a(n, k) + p(n, k)) \right] \quad (23a) \end{aligned}$$

$$\begin{aligned} v^{(i+1)}(n, k) = V_k \left[\alpha(n, k) s(n, k) \right. \\ \left. + 2\mu(b(n, k) + q(n, k)) \right] \quad (23b) \end{aligned}$$

where

$$\alpha(n, k) = \left[\sum_{k=0}^{K-1} V_k \right]^{-1} \left[x(n) - 2\mu \sum_{k=0}^{K-1} \gamma(n, k) \right]$$

$$\gamma(n, k) = V_k \left[c(n, k)(a(n, k) + p(n, k)) \right]$$

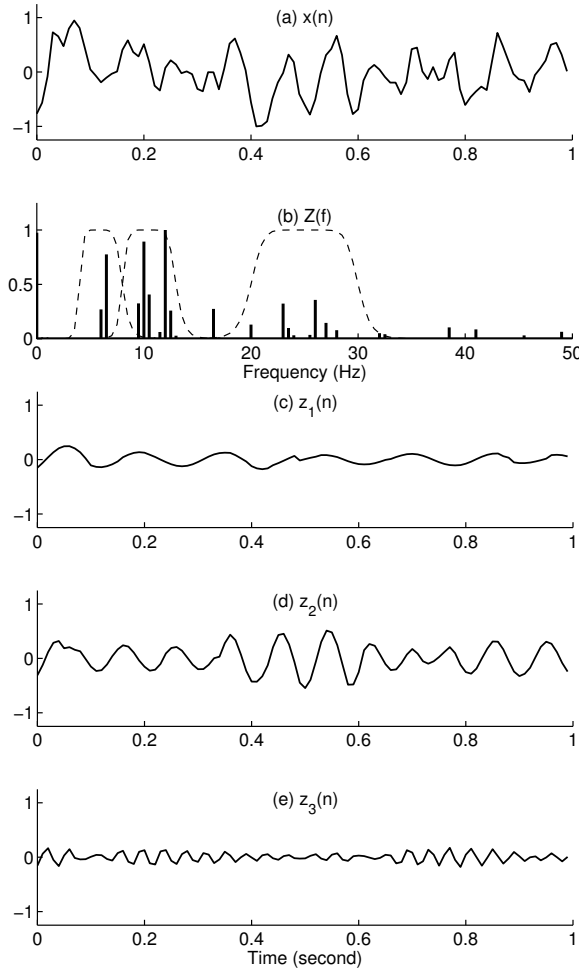


Fig. 5. Example 2: EEG signal, sparse frequency spectrum obtained using sparse frequency analysis (SFA), band-pass components reconstructed from SFA decomposition.

$$+ s(n, k)(b(n, k) + q(n, k)) \quad (24)$$

and

$$V_k = \frac{\Lambda_k^{(i)}}{2\mu\Lambda_k^{(i)} + \lambda} \quad (25)$$

for $n \in \mathbb{Z}_N$, $k \in \mathbb{Z}_K$. Equations (21) and (23) constitute an MM algorithm for computing the solution to (16b). Numerous MM iterations are required in order to obtain an accurate solution to (16b). However, due to the nesting of the MM algorithm within the ADMM algorithm, it is not necessary to perform many MM iterations for each ADMM iteration.

C. Example 2: EEG Signal

An electroencephalogram (EEG) is the measurement of electrical activity of the brain. Several frequency bands have been recognized as having physiological significance, for example: $4 \leq f \leq 8$ Hz (theta rhythms), $8 \leq f \leq 13$ Hz (alpha rhythms), $13 \leq f \leq 30$ Hz (beta rhythms). These rhythms are usually obtained by band-pass filtering EEG data [50].

A one-second EEG signal from [50], with sampling rate $f_s = 100$ Hz, is illustrated in Fig. 5. In this example, we aim

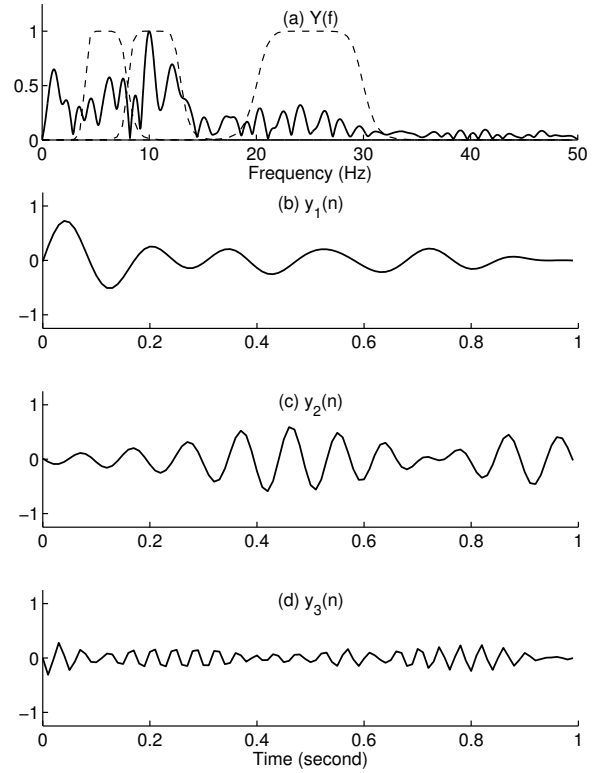


Fig. 6. Example 2: Fourier transform of EEG signal and band-pass components obtained using LTI band-pass filtering.

to estimate the three noted rhythms via the proposed sparse frequency analysis method, and compare the result with that of band-pass filtering.

The proposed method yields the sparse frequency spectrum illustrated in Fig. 5. In order to implement (non-linear) band-pass filtering using the proposed method, we simply reconstruct the signal by weighting each frequency component by the frequency response of a specified band-pass filter,

$$g_H(n) = \sum_{k \in \mathbb{Z}_K} |H(f_k)| (a(n, k) c(n, k) + b(n, k) s(n, k)).$$

This generalization of (13) incorporates the frequency response of the band-pass filter, H .

Three band-pass filters H_i , $i = 1, 2, 3$, are designed according to the theta, alpha, and beta rhythms. Their frequency responses are illustrated in Fig. 5, overlaid on the sparse spectrum obtained by the proposed technique. The three reconstructed components g_{H_i} are illustrated in Fig. 5. It can be seen that each component has relatively piecewise-constant amplitudes and phases. For example, the component g_{H_1} in Fig. 5(c) exhibits an amplitude/phase discontinuity at about $t = 0.5$ seconds. The component g_{H_2} in Fig. 5(d) exhibits an amplitude/phase discontinuity at about $t = 0.35$ seconds and shortly after $t = 0.6$ seconds. The (instantaneous) amplitude/phase functions are otherwise relatively constant.

The signals obtained by LTI band-pass filtering are shown in Fig. 6. The utilized band-pass filters are those that were used for the sparse frequency approach. The Fourier transform of the EEG signal is shown in Fig. 6(a).

Comparing the estimated theta, alpha, and beta rhythms

obtained by the two methods, shown in Figs. 5 and 6, it can be seen that they are quite similar. Hence, the proposed method gives a result that is reasonably similar to LTI band-pass filtering, as desired. Yet, the proposed approach provides a potentially more accurate estimation of abrupt changes in amplitude and phase. In this example, the true components are, of course, unknown. However, the sparse frequency analysis approach provides an alternative to LTI filtering, useful in particular, where it is thought the underlying components are sparse in frequency and possess sparse amplitude and phase derivatives.

IV. SPARSE FREQUENCY APPROXIMATION

In applications, the available data $y(n)$ is usually somewhat noisy and it may be unnecessary or undesirable to enforce the perfect reconstruction constraint in (P0). Here we assume the data is of the form $\mathbf{y} = \mathbf{x} + \mathbf{w}$, where \mathbf{w} denotes additive white Gaussian noise. In this case, a problem formulation more suitable than (P0) is the following one, where, as in basis pursuit denoising (BPD) [14], an approximate representation of the data is sought.

$$\begin{aligned} & \min_{\mathbf{a}, \mathbf{b}} \sum_{k=0}^{K-1} \left(\|\mathbf{D}\mathbf{a}_k\|_1 + \|\mathbf{D}\mathbf{b}_k\|_1 + \lambda \sqrt{\|\mathbf{a}_k\|_2^2 + \|\mathbf{b}_k\|_2^2} \right) \\ & + \lambda_1 \sum_{n=0}^{N-1} \left[y(n) - \sum_{k=0}^{K-1} \left(a(n, k) c(n, k) + b(n, k) s(n, k) \right) \right]^2 \end{aligned} \quad (\text{P1})$$

The parameter $\lambda_1 > 0$ should be chosen according to the noise level. In the following, we derive an algorithm for solving (P1).

Applying variable splitting, as above, (P1) can be rewritten:

$$\begin{aligned} & \min_{\mathbf{a}, \mathbf{b}, \mathbf{u}, \mathbf{v}} \sum_{k=0}^{K-1} \left(\|\mathbf{D}\mathbf{a}_k\|_1 + \|\mathbf{D}\mathbf{b}_k\|_1 + \lambda \sqrt{\|\mathbf{u}_k\|_2^2 + \|\mathbf{v}_k\|_2^2} \right) \\ & + \lambda_1 \sum_{n=0}^{N-1} \left[y(n) - \sum_{k=0}^{K-1} \left(u(n, k) c(n, k) + v(n, k) s(n, k) \right) \right]^2 \\ & \text{s. t. } \begin{cases} \mathbf{u} = \mathbf{a} \\ \mathbf{v} = \mathbf{b}. \end{cases} \end{aligned}$$

As above, we apply ADMM, to obtain the iterative algorithm:

$$\begin{aligned} \mathbf{a}, \mathbf{b} \leftarrow \arg \min_{\mathbf{a}, \mathbf{b}} \sum_{k=0}^{K-1} \left(\|\mathbf{D}\mathbf{a}_k\|_1 + \|\mathbf{D}\mathbf{b}_k\|_1 \right. \\ \left. + \mu \|\mathbf{u}_k - \mathbf{a}_k - \mathbf{p}_k\|_2^2 + \mu \|\mathbf{v}_k - \mathbf{b}_k - \mathbf{q}_k\|_2^2 \right) \end{aligned} \quad (26a)$$

$$\begin{aligned} \mathbf{u}, \mathbf{v} \leftarrow \arg \min_{\mathbf{u}, \mathbf{v}} \sum_{k=0}^{K-1} \left(\lambda \sqrt{\|\mathbf{u}_k\|_2^2 + \|\mathbf{v}_k\|_2^2} \right. \\ \left. + \mu \|\mathbf{u}_k - \mathbf{a}_k - \mathbf{p}_k\|_2^2 + \mu \|\mathbf{v}_k - \mathbf{b}_k - \mathbf{q}_k\|_2^2 \right) \\ \left. + \lambda_1 \sum_{n=0}^{N-1} \left[y(n) - \sum_{k=0}^{K-1} \left(u(n, k) c(n, k) + v(n, k) s(n, k) \right) \right]^2 \end{aligned} \quad (26b)$$

$$\mathbf{p} \leftarrow \mathbf{p} - (\mathbf{u} - \mathbf{a}) \quad (26c)$$

$$\mathbf{q} \leftarrow \mathbf{q} - (\mathbf{v} - \mathbf{b}) \quad (26d)$$

$$\text{Go to (26a)}. \quad (26e)$$

Note that step (26a) is exactly the same as (16a), the solution of which is given by (18), i.e., TV denoising. To solve (26b) for \mathbf{u} and \mathbf{v} , we use MM with the majorizer given in (20). With this majorizer, an MM algorithm to solve (26b) is given by the following iteration, where i is the MM iteration index.

$$\begin{aligned} & \mathbf{u}^{(i+1)}, \mathbf{v}^{(i+1)} \\ & \leftarrow \arg \min_{\mathbf{u}, \mathbf{v}} \sum_{n=0}^{N-1} \left[\sum_{k=0}^{K-1} \frac{\lambda}{2\Lambda_k^{(i)}} (|u(n, k)|^2 + |v(n, k)|^2) \right. \\ & \left. + \lambda_1 \left(y(n) - \sum_{k=0}^{K-1} (u(n, k) c(n, k) + v(n, k) s(n, k)) \right)^2 \right. \\ & \left. + \mu \sum_{k=0}^{K-1} |u(n, k) - a(n, k) - p(n, k)|^2 \right. \\ & \left. + \mu \sum_{k=0}^{K-1} |v(n, k) - b(n, k) - q(n, k)|^2 \right] \end{aligned} \quad (27)$$

where $\Lambda_k^{(i)}$ is given by (21). As in (22), problem (27) decouples with respect to n and the solution $\mathbf{u}^{(i+1)}, \mathbf{v}^{(i+1)}$ can be found in explicit form:

$$\begin{aligned} u^{(i+1)}(n, k) &= V_k \left[\beta(n, k) c(n, k) + 2\mu(a(n, k) + p(n, k)) \right] \\ v^{(i+1)}(n, k) &= V_k \left[\beta(n, k) s(n, k) + 2\mu(b(n, k) + q(n, k)) \right] \end{aligned}$$

where

$$\begin{aligned} \beta(n, k) &= \left[\frac{1}{2\lambda_1} + \sum_{k=0}^{K-1} V_k \right]^{-1} \left[y(n) - 2\mu \sum_{k=0}^{K-1} \gamma(n, k) \right] \\ \gamma(n, k) &= V_k \left[c(n, k) (a(n, k) + p(n, k)) \right. \\ & \left. + s(n, k) (b(n, k) + q(n, k)) \right] \end{aligned} \quad (28)$$

where V_k is given by (25).

A. Example 3: A Noisy Multiband Signal

This example illustrates the estimation of a sinusoid with a phase discontinuity when the observed data includes numerous other components, including additive white Gaussian noise. The example also illustrates the estimation of the instantaneous phase of the estimated component. The resulting instantaneous phase function is compared with that obtained using a band-pass filter and the Hilbert transform. The Hilbert transform is widely used in applications such as EEG analysis [38], [46], [58], [60].

The one-second signal $x(t)$, with sampling rate of $F_s = 100$ Hz ($N = 100$ samples), illustrated in Fig. 7c, is synthesized as follows: adding the 9.5 Hz sinusoid $r(t)$ (with phase discontinuity at $t = 0.4$ seconds) in Fig. 7a, and the sinusoids and white Gaussian noise illustrated in Fig. 7b. Note that the

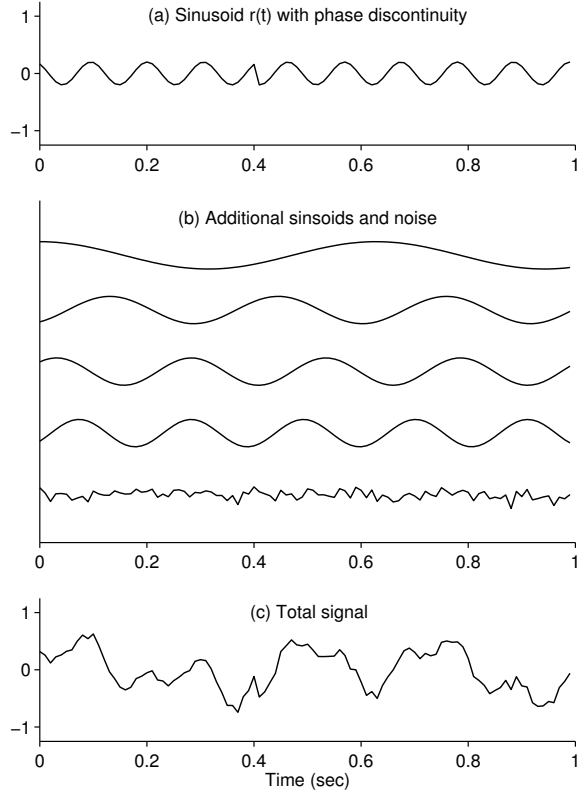


Fig. 7. Example 3: The signal $x(t)$ in (c) is synthesized as the sum of (a) 9.5 Hz sinusoid with a phase discontinuity and (b) additional sinusoids and white Gaussian noise.

instantaneous frequency of $r(t)$ has an impulse at $t = 0.4$ due to the phase discontinuity.

The sparse frequency analysis approach (P1) was solved with the iterative algorithm described above. We used $K = 50$ uniformly spaced frequencies from 0 to 50 Hz, we obtain $\mathbf{a}, \mathbf{b} \in \mathbb{R}^{N \times K}$, the time-varying cosine and sine amplitudes, with discrete frequencies $f_k = k$ Hz. The sparse frequency spectrum is illustrated in Fig. 8(a). Our aim is to recover $r(t)$, but (by design) its frequency of 9.5 Hz is halfway between the discrete frequencies f_9 and f_{10} , which are clearly visible in the sparse spectrum. Hence, an estimate of $r(t)$ is obtained via (13) using the index set $S = \{9, 10\}$, i.e., $\hat{r}(t) = g_{\{9,10\}}(t)$,

$$g_S(t) = a_9(t) \cos \omega_9 t + b_9(t) \sin \omega_9 t + a_{10}(t) \cos \omega_{10} t + b_{10}(t) \sin \omega_{10} t. \quad (29)$$

The time-varying amplitudes, $a_k(t)$ and $b_k(t)$ for $k = 9, 10$, are illustrated in Fig. 8 (dashed lines). Within the same plots, the functions $a_k(t) \cos(\omega_k t)$ and $b_k(t) \sin(\omega_k t)$ with $\omega_k = 2\pi f_k$ for $k = 9, 10$ are also shown (solid lines). The piecewise-constant property of $a_k(t)$ and $b_k(t)$ is clearly visible. The signal $g_S(t)$ is also illustrated in the figure. Note that $g_S(t)$ has a center frequency of 9.5 Hz, while the sinusoids from which it is composed have frequencies 9 and 10 Hz.

To compute and analyze the instantaneous phase of the signal $g_S(t)$, it is convenient to express $g_S(t)$ in terms of a single frequency (9.5 Hz) instead of two distinct frequencies (9 and 10 Hz). Therefore, by trigonometric identities, we write

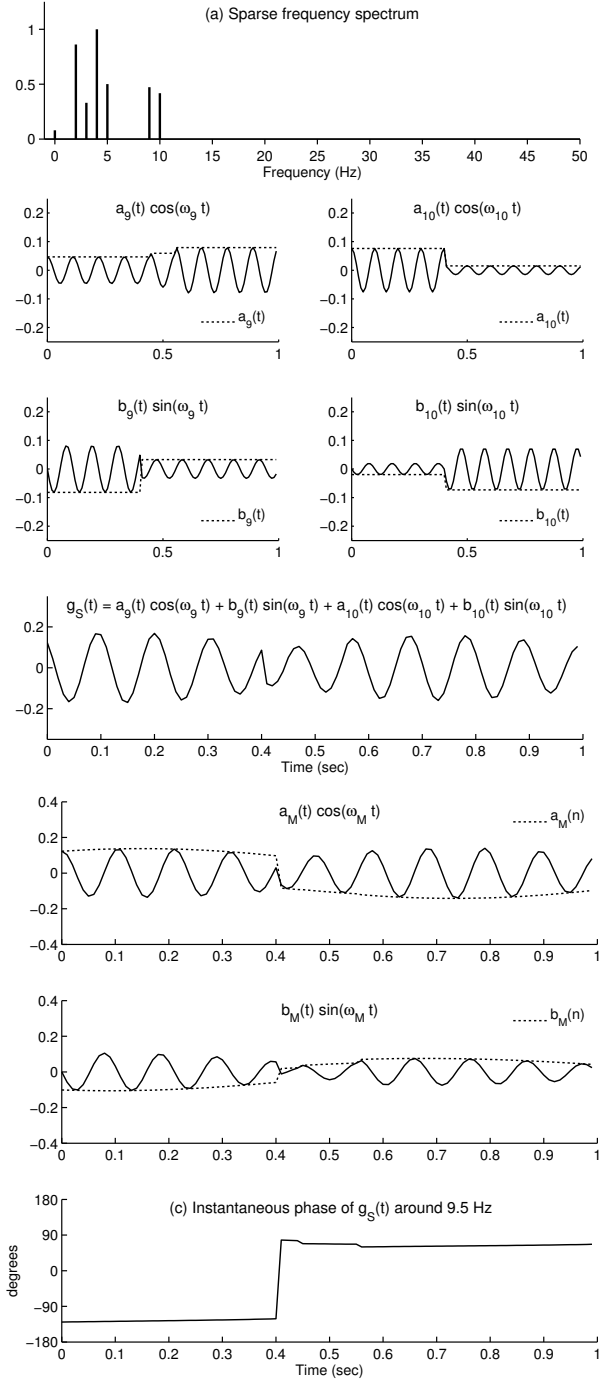


Fig. 8. Example 3: Signal decomposition using sparse frequency analysis (SFA). The discontinuity in the instantaneous phase of the 9.5 Hz sinusoid is accurately recovered.

$$g_S(t) = a_m(t) \cos(\omega_m t) + b_m(t) \sin(\omega_m t) + a_{m+1}(t) \cos(\omega_{m+1} t) + b_{m+1}(t) \sin(\omega_{m+1} t) \quad (30)$$

as

$$g_S(t) = a_M(t) \cos(\omega_M t) + b_M(t) \sin(\omega_M t) \quad (31)$$

where

$$a_M(t) = (a_m(t) + a_{m+1}(t)) \cos(\Delta\omega t) - (b_m(t) - b_{m+1}(t)) \sin(\Delta\omega t) \quad (32)$$

$$b_M(t) = (b_m(t) + b_{m+1}(t)) \cos(\Delta\omega t) - (a_m(t) - a_{m+1}(t)) \sin(\Delta\omega t) \quad (33)$$

and

$$\omega_M = (\omega_m + \omega_{m+1})/2, \quad \Delta\omega = (\omega_{m+1} - \omega_m)/2.$$

Here ω_M is the frequency midway between ω_m and ω_{m+1} . Equation (31) expresses $g_S(t)$ in terms of a single center frequency, ω_M , instead of two distinct frequencies as in (30). Note that $a_M(t)$ and $b_M(t)$ are readily obtained from the time varying amplitudes $a_k(t)$ and $b_k(t)$. The functions $a_M(t) \cos(\omega_M t)$ and $b_M(t) \sin(\omega_M t)$ are illustrated in Fig. 8, where $a_M(t)$ and $b_M(t)$ are shown as dashed lines. Note that these amplitude functions are piecewise smooth (not piecewise constant), due to the $\cos(\Delta\omega t)$ and $\sin(\Delta\omega t)$ terms.

To obtain an instantaneous phase function from (31) it is furthermore convenient to express $g_S(t)$ in terms of $M(t) \exp(j\omega_M t)$. To that end, we write $g_S(t)$ as

$$g_S(t) = \frac{1}{2} a_M(t) e^{j\omega_M t} + \frac{1}{2} a_M(t) e^{-j\omega_M t} + \frac{1}{2j} b_M(t) e^{j\omega_M t} - \frac{1}{2j} b_M(t) e^{-j\omega_M t} \quad (34)$$

or

$$g_S(t) = \left[\frac{1}{2} a_M(t) + \frac{1}{2j} b_M(t) \right] e^{j\omega_M t} + \left[\frac{1}{2} a_M(t) - \frac{1}{2j} b_M(t) \right] e^{-j\omega_M t} \quad (35)$$

which we write as

$$g_S(t) = \frac{1}{2} g_+(t) e^{j\omega_M t} + \frac{1}{2} [g_+(t)]^* e^{-j\omega_M t} \quad (36)$$

where $g_+(t)$ is the ‘positive frequency’ component, defined as

$$g_+(t) := a_M(t) + \frac{1}{j} b_M(t). \quad (37)$$

According to the model assumptions, $g_+(t)$ is expected to be piecewise smooth with the exception of sparse discontinuities. We can use (37) to define the instantaneous phase function

$$\theta_M(t) = -\tan^{-1} \left(\frac{b_M(t)}{a_M(t)} \right). \quad (38)$$

The function $\theta_M(t)$ represents the deviation of $g_S(t)$ around its center frequency, ω_M . It is useful to use the four-quadrant arctangent function for (38), i.e., ‘atan2’. For the current example, the instantaneous phase $\theta_M(t)$ for the 9.5 Hz signal, $g_S(t)$, is illustrated in Fig. 8. It clearly shows a discontinuity at $t = 0.4$ of about 180 degrees.

A finer frequency discretization would also be effective here to reduce the issue of the narrow-band signal component (9.5 Hz) falling between discrete frequencies (9 and 10 Hz). However, an aim of this example is to demonstrate how this case is effectively handled when using sparse frequency analysis (SFA).

The estimate of the 9.5 Hz signal $r(t)$ obtained by band-pass filtering is illustrated in Fig. 9a (solid line). The utilized band-pass filter was designed to pass frequencies 8–12 Hz (i.e., alpha rhythms). The Hilbert transform is also shown

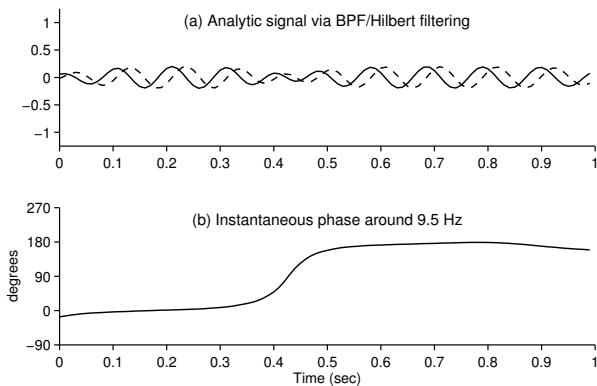


Fig. 9. Example 3: The estimate of the 9.5 Hz component using LTI band-pass filtering. The instantaneous phase, computed using the Hilbert transform, exhibits a gradual phase shift.

(dashed line). The instantaneous phase of the analytic signal (around 9.5 Hz) is illustrated in Fig. 9b. It can be seen that the instantaneous phase undergoes a 180 degree shift around $t = 0.4$ seconds, but the transition is not sharp. Given a real-valued signal $y(t)$, a complex-valued analytic signal $y_a(t)$ is formed by $y_a(t) = y(t) + j y_H(t)$, where $y_H(t)$ is the Hilbert transform of $y(t)$.

In contrast with LTI filtering (band-pass filter and Hilbert transform), the sparse frequency analysis (SFA) method yields an instantaneous phase function that accurately captures the step discontinuity at $t = 0.4$. Hence, unlike LTI filtering, the sparse frequency analysis (SFA) approach makes possible the high resolution estimation of phase discontinuities of a narrow-band signal buried within a noisy multi-band signal. This is true even when the center frequency of the narrow-band signal falls between the discrete frequencies f_k .

V. MEASURING PHASE SYNCHRONY

The study of synchronization of various signals is of interest in biology, neuroscience, and in the study of the dynamics of physical systems [33], [47]. Phase synchrony is a widely utilized form of synchrony, which is thought to play a role in the integration of functional areas of the brain, in associative memory, and motor planning, etc. [33], [57], [59]. Phase synchrony is often quantified by the *phase locking value* (PLV). Various methods for quantifying, estimating, extending, and using phase synchrony have been developed [5], [6], [28].

The phase synchrony between two signals is meaningfully estimated when each signal is approximately narrow-band. Therefore, methods to measure phase synchrony generally utilize band-pass filters designed to capture the frequency band of interest. Generally, the Hilbert transform is then used to compute a complex analytic signal from which the time-varying phase is obtained. In this example, we illustrate the use of SFA for estimating the instantaneous phase difference between two channels of a multichannel EEG.

A. Example 4: EEG instantaneous phase difference

Two channels of an EEG, with sampling rate $f_s = 200$ Hz, are shown in Fig. 10. Band-pass signals in the 11–15 Hz band,

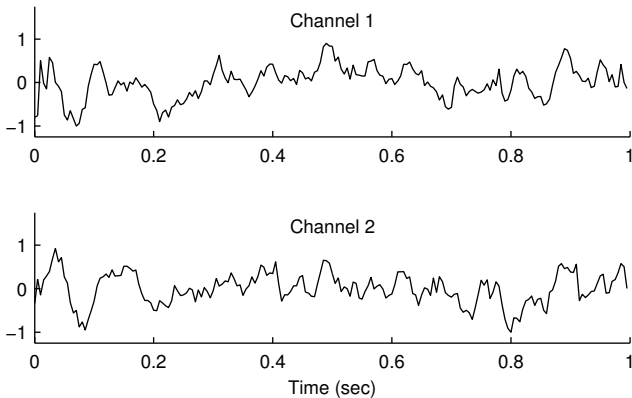


Fig. 10. Example 4: Two channels of a multichannel EEG signal.

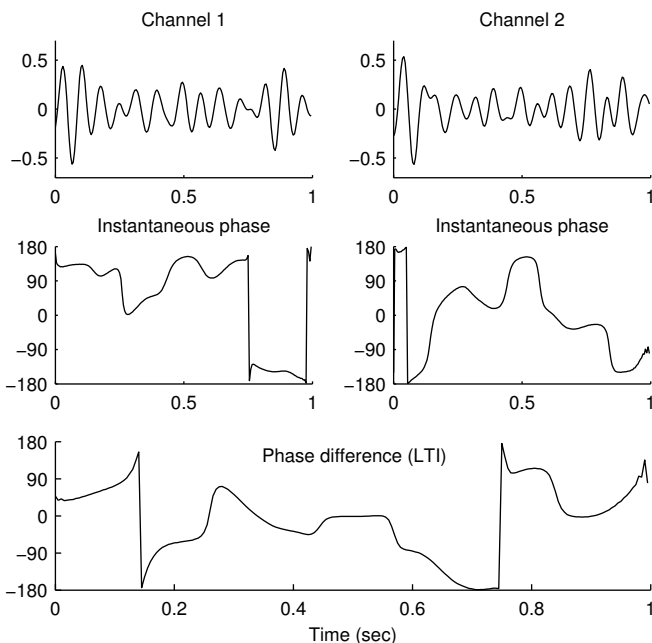


Fig. 11. Example 4: Band-pass (11-15 Hz) signals estimated using LTI band-pass filtering. Instantaneous phase functions obtained using Hilbert transform. Channel 1 (left) and channel 2 (right). Bottom: instantaneous phase difference.

obtained via band-pass filtering are illustrated in Fig. 11. The instantaneous phase functions (around 13 Hz) are computed using the Hilbert transform, and the phase difference is shown. The computation of the phase locking value (PLV) and other phase-synchronization indices are based on the difference of the instantaneous phase functions.

The sparse frequency analysis (SFA) technique provides an alternative approach to obtain the instantaneous phase of each channel of the EEG and the phase difference function. Phase synchronization indices can be subsequently calculated, as they are when the instantaneous phase difference is computed via LTI filtering. Here we use problem formulation (P0) with $K = 100$, with the frequencies f_k , equally spaced from 0 to 99 Hz, i.e., $f_k = k$ Hz, $0 \leq k \leq K - 1$. With this frequency grid, the 11–15 Hz band corresponds to five frequency components, i.e. $k \in S = \{11, \dots, 15\}$. The 11-15 Hz band can then be identified as $g_S(t)$ in (13).

In order to compute the instantaneous phase of $g_S(t)$, we express $g_S(t)$ in terms of sines/cosines with time-varying amplitudes and constant frequency as in (31). For this purpose, we write $g_S(t)$ as

$$g_S(t) = g_{\{11,15\}}(t) + g_{\{12,14\}}(t) + g_{\{13\}}(t). \quad (39)$$

Using (32) and (33), we can write

$$g_{\{13\}}(t) = a_M^{(0)}(t) \cos(\omega_M t) + b_M^{(0)}(t) \sin(\omega_M t) \quad (40)$$

$$g_{\{12,14\}}(t) = a_M^{(1)}(t) \cos(\omega_M t) + b_M^{(1)}(t) \sin(\omega_M t) \quad (41)$$

$$g_{\{11,15\}}(t) = a_M^{(2)}(t) \cos(\omega_M t) + b_M^{(2)}(t) \sin(\omega_M t) \quad (42)$$

where $\omega_M = 2\pi f_{13} = 26\pi$, with f_{13} being the middle of the five frequencies in S . The functions $a_M^{(i)}(t)$, $b_M^{(i)}(t)$ are obtained by (32) and (33) from the amplitude functions $a_k(t)$, $b_k(t)$ produced by SFA. Therefore, we can write the 11-15 Hz band signal, $g_S(t)$, as (31) where

$$a_M(t) = a_M^{(0)}(t) + a_M^{(1)}(t) + a_M^{(2)}(t) \quad (43)$$

$$b_M(t) = b_M^{(0)}(t) + b_M^{(1)}(t) + b_M^{(2)}(t). \quad (44)$$

Further, the instantaneous phase of $g_S(t)$ can be obtained using (38). The 11-15 Hz band of each of the two EEG channels so obtained via SFA, and their instantaneous phase functions, are illustrated in Fig. 12.

Comparing the phase difference functions obtained by SFA and BPF/Hilbert (LTI) filtering, it can be noted that they are quite similar but the phase difference estimated by SFA is somewhat more stable. Between 0.3 and 0.4 seconds, the SFA phase-difference varies less than the LTI phase-difference. Moreover, in the interval between 0.15 and 0.2 seconds, the LTI phase difference is increasing, while for SFA it is decreasing.

The true underlying subband signals are unknown; yet, if they do possess abrupt amplitude/phase transitions, the SFA technique may represent them more accurately. In turn, SFA, may provide more precise timing of phase locking/unlocking.

VI. CONCLUSION

This paper describes a sparse frequency analysis (SFA) method by which an N -point discrete-time signal $x(n)$ can be expressed as the sum of sinusoids wherein the amplitude and phase of each sinusoid is a time-varying function. In particular, the amplitude and phase of each sinusoid is modeled as being approximately piecewise constant (i.e., the temporal derivatives of the instantaneous amplitude and phase functions are modeled as sparse). The signal $x(n)$ is furthermore assumed to have a sparse frequency spectrum so as to make the representation well posed. The SFA method can be interpreted as a generalization of the discrete Fourier transform (DFT), since, highly regularizing the temporal variation of the amplitudes of the sinusoidal components leads to a solution wherein the amplitudes are non-time-varying.

The SFA method, as described here, is defined by a convex optimization problem, wherein the total variation (TV) of the sine/cosine amplitude functions, and the frequency spectrum are regularized, subject to either a perfect or approximate reconstruction constraint. An iterative algorithm is derived

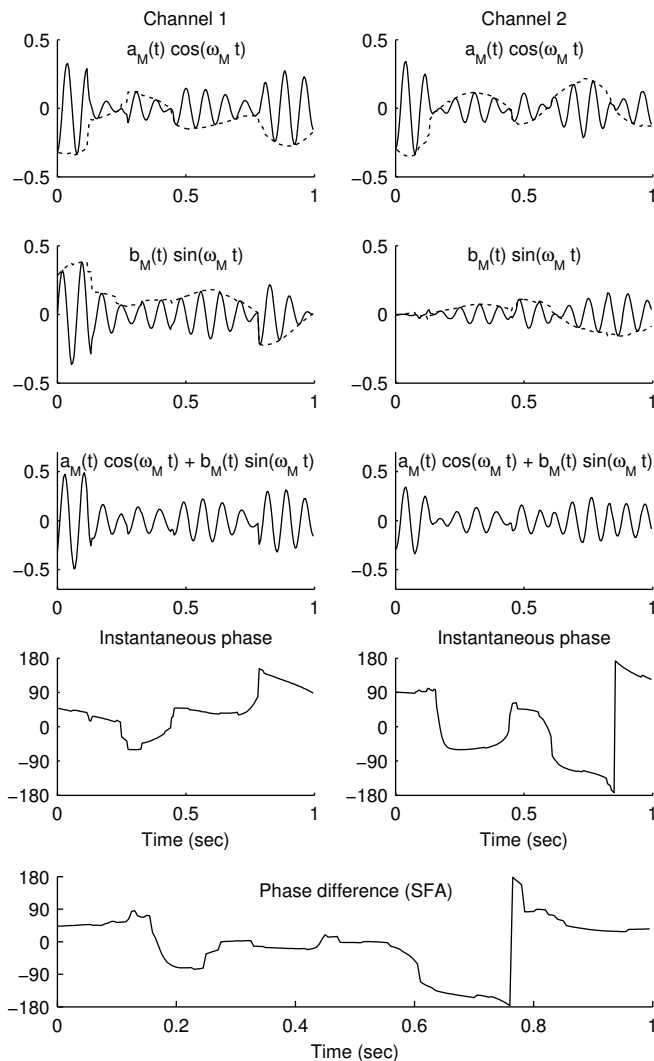


Fig. 12. Example 4: Band-pass (11-15 Hz) signals estimated using sparse frequency analysis (SFA). Channel 1 (left) and channel 2 (right). Bottom: instantaneous phase difference.

using variable splitting, ADMM, and MM techniques from convex optimization. Due to the convexity of the formulated optimization problem and the properties of ADMM, the algorithm converges reliably to the unique optimal solution.

Examples showed that the SFA technique can be used to perform mildly non-linear band-pass filtering so as to extract a narrow-band signal from a wide-band signal, even when the narrow-band signal exhibits amplitude/phase jumps. This is in contrast to conventional linear time-invariant (LTI) filtering which spreads amplitude/phase discontinuities across time and frequency. The SFA method is illustrated using both synthetic signals and human EEG data.

Several extensions of the presented SFA method are envisioned. For example, depending on the data, a non-convex formulation that more strongly promotes sparsity may be suitable. Methods such as re-weighted L1 or L2 norm minimization [10], [26], [63] or greedy algorithms [36] can be used to address the non-convex form of SFA. In addition, instead of modeling the frequency components as being approximately piecewise

constant, it will be of interest to model them as being piecewise smooth. In this case, the time-varying amplitude functions may be regularized using generalized or higher-order total variation [8], [29], [32], [53], or a type of wavelet transform [9]. Incorporating higher-order TV into the proposed SFA framework is an interesting avenue for further study.

REFERENCES

- [1] O. Adam. Advantages of the Hilbert Huang transform for marine mammals signals analysis. *J. Acoust. Soc. Am.*, 120:2965–2973, 2006.
- [2] M. V. Afonso, J. M. Bioucas-Dias, and M. A. T. Figueiredo. Fast image recovery using variable splitting and constrained optimization. *IEEE Trans. Image Process.*, 19(9):2345–2356, September 2010.
- [3] M. V. Afonso, J. M. Bioucas-Dias, and M. A. T. Figueiredo. An augmented Lagrangian approach to the constrained optimization formulation of imaging inverse problems. *IEEE Trans. Image Process.*, 20(3):681–695, March 2011.
- [4] J. B. Allen and L. R. Rabiner. A unified approach to short-time Fourier analysis and synthesis. *Proc. IEEE*, 65(11):1558–1564, November 1977.
- [5] M. Almeida, J. H. Schleimer, J. M. Bioucas-Dias, and R. Vigarrio. Source separation and clustering of phase-locked subspaces. *IEEE Trans. Neural Networks*, 22(9):1419–1434, September 2011.
- [6] S. Aviyente and A. Y. Mutlu. A time-frequency-based approach to phase and phase synchrony estimation. *IEEE Trans. Signal Process.*, 59(7):3086–3098, July 2011.
- [7] S. Boyd, N. Parikh, E. Chu, B. Peleato, and J. Eckstein. Distributed optimization and statistical learning via the alternating direction method of multipliers. *Foundations and Trends in Machine Learning*, 3(1):1–122, 2011.
- [8] K. Bredies, K. Kunisch, and T. Pock. Total generalized variation. *SIAM J. Imag. Sci.*, 3(3):492–526, 2010.
- [9] C. S. Burrus, R. A. Gopinath, and H. Guo. *Introduction to Wavelets and Wavelet Transforms*. Prentice Hall, 1997.
- [10] E. J. Candès, M. B. Wakin, and S. Boyd. Enhancing sparsity by reweighted l1 minimization. *J. Fourier Anal. Appl.*, 14(5):877–905, December 2008.
- [11] A. Chambolle. An algorithm for total variation minimization and applications. *J. of Math. Imaging and Vision*, 20:89–97, 2004.
- [12] T. F. Chan, S. Osher, and J. Shen. The digital TV filter and nonlinear denoising. *IEEE Trans. Image Process.*, 10(2):231–241, February 2001.
- [13] R. Chartrand and V. Staneva. Total variation regularization of images corrupted by non-Gaussian noise using a quasi-Newton method. *Image Processing, IET*, 2(6):295–303, December 2008.
- [14] S. Chen, D. L. Donoho, and M. A. Saunders. Atomic decomposition by basis pursuit. *SIAM J. Sci. Comput.*, 20(1):33–61, 1998.
- [15] P. L. Combettes and J.-C. Pesquet. Proximal splitting methods in signal processing. In H. H. Bauschke et al., editors, *Fixed-Point Algorithms for Inverse Problems in Science and Engineering*. Springer-Verlag, 2010.
- [16] L. Condat. A direct algorithm for 1D total variation denoising. Technical report, Hal-00675043, 2012. <http://hal.archives-ouvertes.fr/>.
- [17] I. Daubechies, J. Lu, and H.-T. Wu. Synchrosqueezed wavelet transforms: An empirical mode decomposition-like tool. *J. of Appl. and Comp. Harm. Analysis*, 30(2):243–261, March 2011.
- [18] P. Derambure, L. Defebvre, K. Dujardin, J. L. Bourriez, J. M. Jacquesson, A. Destee, and J. D. Guieu. Effect of aging on the spatio-temporal pattern of event-related desynchronization during a voluntary movement. *Electroencephalography and Clinical Neurophysiology Evoked Potentials Section*, 89(3):197–203, 1993.
- [19] S. Durand and J. Froment. Reconstruction of wavelet coefficients using total variation minimization. *SIAM J. Sci. Comput.*, 24(5):1754–1767, 2003.
- [20] M. Figueiredo, J. Bioucas-Dias, J. P. Oliveira, and R. D. Nowak. On total-variation denoising: A new majorization-minimization algorithm and an experimental comparison with wavelet denoising. In *Proc. IEEE Int. Conf. Image Processing*, 2006.
- [21] M. Figueiredo, J. M. Bioucas-Dias, and R. Nowak. Majorization-minimization algorithms for wavelet-based image restoration. *IEEE Trans. Image Process.*, 16(12):2980–2991, December 2007.
- [22] P. Flandrin and P. Goncalves. Empirical mode decompositions as data-driven wavelet-like expansions. *Int. J. Wavelets Multires. Inf. Process.*, 2(4):477496, 2004.
- [23] S. A. Fulop and K. Fitz. Algorithms for computing the time-corrected instantaneous frequency (reassigned) spectrogram, with applications. *J. Acoust. Soc. Am.*, 119(1):360–371, January 2006.

- [24] F. Gianfeli, G. Biagetti, P. Crippa, and C. Turchetti. Multicomponent AM-FM representations: An asymptotically exact approach. *IEEE Trans. Audio, Speech, and Lang. Proc.*, 15(3):823–837, March 2007.
- [25] F. Gianfeli, C. Turchetti, and P. Crippa. Multicomponent AM-FM demodulation: The state of the art after the development of the iterated Hilbert transform. In *IEEE Int. Conf. Sig. Proc. Comm. (ICSPC)*, pages 1471–1474, November 2007.
- [26] I. F. Gorodnitsky and B. D. Rao. Sparse signal reconstruction from limited data using FOCUSS: a re-weighted minimum norm algorithm. *IEEE Trans. Signal Process.*, 45(3):600–616, March 1997.
- [27] T. Y. Hou and Z. Shi. Adaptive data analysis via sparse time-frequency representation. *Adv. Adaptive Data Analysis*, 03(1-2):1–28, 2011.
- [28] S. Hu, M. Stead, Q. Dai, and G. A. Worrell. On the recording reference contribution to EEG correlation, phase synchrony, and coherence. *IEEE Trans. Systems, Man., and Cybernetics, Part B: Cybernetics.*, 40(5):1294–1304, October 2010.
- [29] Y. Hu and M. Jacob. Higher degree total variation (HDTV) regularization for image recovery. *IEEE Trans. Image Process.*, 21(5):2559–2571, May 2012.
- [30] N. E. Huang, Z. Shen, S. R. Long, M. C. Wu, H. H. Shih, Q. Zheng, N. C. Yen, C. C. Tung, and H. H. Liu. The empirical mode decomposition and Hilbert spectrum for nonlinear and non-stationary time series analysis. *Proc. Roy. Soc. Lon. A*, 454:903–995, March 1998.
- [31] J. Kalcher and G. Pfurtscheller. Discrimination between phase-locked and non-phase-locked event-related EEG activity. *Electroencephalography and Clinical Neurophysiology*, 94(5):381–384, 1995.
- [32] F. I. Karahanoglu, I. Bayram, and D. Van De Ville. A signal processing approach to generalized 1-d total variation. *IEEE Trans. Signal Process.*, 59(11):5265–5274, November 2011.
- [33] J. Lachaux, E. Rodriguez, J. Martinerie, and F. J. Varela. Measuring phase synchrony in brain signals. *Hum. Brain Mapp*, 8:194–208, 1999.
- [34] P. Loughlin, J. Pittona, and B. Hannaford. Approximating time-frequency density functions via optimal combinations of spectrograms. *IEEE Signal Processing Letters*, 1(12):199–202, December 1994.
- [35] M. W. Macon and M. A. Clements. Sinusoidal modeling and modification of unvoiced speech. *IEEE Trans. Acoust., Speech, Signal Proc.*, 5(6):557–560, November 1997.
- [36] S. Mallat and Z. Zhang. Matching pursuits with time-frequency dictionaries. *IEEE Trans. Signal Process.*, 41:3397–3415, December 1993.
- [37] R. McAulay and T. Quatieri. Speech analysis/synthesis based on a sinusoidal representation. *IEEE Trans. Acoust., Speech, Signal Proc.*, 34(4):744–754, August 1986.
- [38] A. Medl, D. Flotzinger, and G. Pfurtscheller. Hilbert-transform based predictions of hand movements from EEG measurements. In *Proc. EMBC*, volume 6, pages 2539–2540, November 1992.
- [39] S. Meignen and V. Perrier. A new formulation for empirical mode decomposition based on constrained optimization. *IEEE Trans. Signal Process.*, 14(12):932–935, December 2007.
- [40] T. Oberlin, S. Meignen, and V. Perrier. An alternative formulation for the empirical mode decomposition. *IEEE Trans. Signal Process.*, 60(5):2236–2246, May 2012.
- [41] J. Oliveira, J. Bioucas-Dias, and M. A. T. Figueiredo. Adaptive total variation image deblurring: A majorization-minimization approach. *Signal Processing*, 89(9):1683–1693, September 2009.
- [42] S. Osher, M. Burger, D. Goldfarb, J. Xu, and W. Yin. An iterative regularization method for total variation based image restoration. *Multiscale Model. & Simul.*, 4(2):460–489, 2005.
- [43] Y. Pantazis, O. Rosenc, and Y. Stylianou. Iterative estimation of sinusoidal signal parameters. *IEEE Signal Processing Letters*, 17(5):461–464, May 2010.
- [44] Y. Pantazis and Y. Stylianou. Improving the modeling of the noise part in the harmonic plus noise model of speech. In *Proc. ICASSP*, pages 4609–4612, April 2008.
- [45] S. Peng and W.-L. Hwang. Null space pursuit: An operator-based approach to adaptive signal separation. *IEEE Trans. Signal Process.*, 58(5):2475–2483, May 2010.
- [46] Y. Periklis and N. Papp. Instantaneous envelope and phase extraction from real signals: Theory, implementation, and an application to EEG analysis. *Signal Processing*, 2(4):373–385, 1980.
- [47] A. Pikovsky, M. Rosenblum, and J. Kurths. *Synchronization: A Universal Concept in Nonlinear Sciences*. Cambridge Nonlinear Science Series. Cambridge University Press, 2003.
- [48] J. W. Pitton, K. Wang, and B. H. Juang. Time-frequency analysis and auditory modeling for automatic recognition of speech. In *Proc. IEEE*, volume 84, pages 1199–1215, September 1996.
- [49] N. Pustelnik, P. Borgnat, and P. Flandrin. A multicomponent proximal algorithm for empirical mode decomposition. In *Proc. Euro. Sig. Proc. Conf. (EUSIPCO)*, pages 1880–1884, August 2012.
- [50] R. M. Rangayyan. *Biomedical Signal Analysis - A Case-study Approach*. IEEE and Wiley, New York, NY, 2002.
- [51] G. Rilling and P. Flandrin. One or two frequencies? The empirical mode decomposition answers. *IEEE Trans. Signal Process.*, 56(1):85–95, 2008.
- [52] G. Rilling, P. Flandrin, and P. Goncalves. On empirical mode decomposition and its algorithms. In *IEEE/EURASIP Workshop on Nonlinear Signal and Image Processing (NSIP)*, 2003.
- [53] P. Rodríguez and B. Wohlberg. Efficient minimization method for a generalized total variation functional. *IEEE Trans. Image Process.*, 18(2):322–332, February 2009.
- [54] L. Rudin, S. Osher, and E. Fatemi. Nonlinear total variation based noise removal algorithms. *Physica D*, 60:259–268, 1992.
- [55] G. Steidl, J. Weickert, T. Brox, P. Mrázek, and M. Welk. On the equivalence of soft wavelet shrinkage, total variation diffusion, total variation regularization, and SIDes. *SIAM J. Numer. Anal.*, 42:686–713, 2004.
- [56] P. A. Tass. *Phase Resetting in Medicine and Biology*. Springer, 2007.
- [57] G. Tononi and G. M. Edelman. Consciousness and complexity. *Science*, 282(5395):1846–1851, 1998.
- [58] S. Vairavan, H. Eswaran, N. Haddad, D. F. Rose, H. Preissl, J. D. Wilson, C. L. Lowery, and R. B. Govindan. Detection of discontinuous patterns in spontaneous brain activity of neonates and fetuses. *IEEE Trans. Biomed. Eng.*, 56(11):2725–2729, November 2009.
- [59] F. J. Varela. Resonant cell assemblies: a new approach to cognitive functions and neuronal synchrony. *Biological Research*, 28(1):81–95, 1995.
- [60] M. Wacker, M. Galicki, P. Putsche, T. Milde, K. Schwab, J. Haueisen, C. Ligges, and H. Witte. A time-variant processing approach for the analysis of alpha and gamma MEG oscillations during flicker stimulus generated entrainment. *IEEE Trans. Biomed. Eng.*, 58(11):3069–3077, November 2011.
- [61] Y. Wang, J. Yang, W. Yin, and Y. Zhang. A new alternating minimization algorithm for total variation image reconstruction. *SIAM J. on Imaging Sciences*, 1(3):248–272, 2008.
- [62] Y. Wang and H. Zhou. Total variation wavelet-based medical image denoising. *Int. J. of Biomedical Imaging*, pages 1–6, 2006. Article ID 89095.
- [63] D. Wipf and S. Nagarajan. Iterative reweighted ℓ_1 and ℓ_2 methods for finding sparse solutions. *IEEE. J. Sel. Top. Signal Processing*, 4(2):317–329, April 2010.
- [64] H. Wu, P.-L. Lee, H.-C. Chang, and J.-C. Hsieh. Accounting for phase drifts in SSVEP-based BCIs by means of biphasic stimulation. *IEEE Trans. Biomed. Eng.*, 58(5):1394–1402, May 2011.
- [65] Y. Xu, S. Haykin, and R. J. Racine. Multiple window time-frequency distribution and coherence of EEG using Slepian sequences and Hermite functions. *IEEE Trans. Biomed. Eng.*, 46(7):861–866, July 1999.